Solid State Science and Technology, Vol. 33, No. 2 (2025) 138-148
https://doi.org/10.66514/ssst33-2-138-148

Immersion-Time-Controlled Growth of $Cu(OH)_2$ Microneedle Arrays on Copper Mesh for Superhydrophobic Oil-Water Separation

Malia Athirah Badruddin[1,2], Nur Adam Zikry Nur Mizhuari[2], Fareed Nordin[2], Mohd Sabri Mohd Ghazali[2], Oon Jew Lee[2,*]

[1]*STEM Foundation Centre, Universiti Malaysia Terengganu, Kuala Nerus 21030 Terengganu, Malaysia*
[2]*Advanced Nano Materials (ANoMa) Research Interest Group, Faculty of Science and Marine Environment, Universiti Malaysia Terengganu, Kuala Nerus 21030 Terengganu, Malaysia*

**Corresponding author (email: oonjew@umt.edu.my)*

(Received: 2 December 2025 / Revised: 2 January 2026 / Accepted: 5 January 2026 / Published online: 7 January 2026)

ABSTRACT

Industrial wastewater, particularly from oil refining, presents serious environmental challenges. It contains oil, grease, and other contaminants that can disrupt water quality and threaten aquatic ecosystems. This research explores the fabrication of a $Cu(OH)_2$-coated copper mesh for oil-water separation by tailoring surface morphology and wettability. $Cu(OH)_2$ needle-like arrays were synthesized on Cu mesh via a facile chemical immersion process. The resulting high-aspect-ratio microstructures significantly altered surface roughness, thereby enhancing hydrophobicity and oleophilicity. A water contact angle of 155.75° and an oil contact angle of 17.52° were achieved for the optimised sample. As a result, oil-water separation efficiencies of 92.77%, 96.20%, 94.46%, and 98.10% were obtained for engine oil, diesel, olive oil, and cyclohexane, respectively. The highest permeation flux of 1648.65 $kg \cdot h^{-1} \cdot m^{-2}$ was observed for cyclohexane, attributed to its low viscosity. The results demonstrate that morphology-controlled $Cu(OH)_2$ microstructures can provide an effective and scalable route for oil-water separation without additional surface chemical modification.

Keywords: Copper mesh; high aspect ratio array; oil-water separation; oleophilic; superhydrophobic

INTRODUCTION

Oily wastewater poses a persistent threat to ecosystems and human health, underscoring the urgent need for efficient and reliable treatment technologies. Conventional separation methods often face limitations in achieving effective oil removal, particularly for oils with varying viscosities. In this context, metal meshes such as stainless steel, copper (Cu),

titanium (Ti), and nickel (Ni) meshes have attracted considerable attention for oil-water separation applications [1,2].

Among these materials, Cu mesh offers a compelling balance between oil-water separation performance and practical usage, owing to its high surface reactivity, corrosion resistance, mechanical flexibility, and tuneable pore size [3,4]. Its high surface reactivity facilitates interfacial wettability coating, imparting hydrophobic (water-repelling) and oleophilic (oil-attracting) characteristics. In addition, Cu mesh exhibits good stability in moderately corrosive environments. Its mechanical flexibility and adjustable pore size further enable optimisation of oil penetration and separation efficiency across different droplet sizes.

Selective oil-water separation is predominantly governed by interfacial wettability, which can be effectively regulated through micro- and nanoscale surface modification. Such structured surfaces act as selective barriers, repelling water while allowing oil to permeate freely. The high surface reactivity of Cu mesh enables the in-situ growth of hierarchical micro- and nanostructures, thereby enhancing surface roughness. However, previous studies have demonstrated that Cu meshes modified solely with rough microstructures, such as nanoneedles [5, 6], nanowires [7, 8], and nanorods [9, 10]. However, the modified meshes often exhibit hydrophilic behaviour. This indicates that surface morphology alone does not always guarantee hydrophobicity.

To overcome this limitation, various fabrication strategies have been developed to tailor hierarchical micro- and nanostructures on Cu meshes, including sol–gel processing [11], electrodeposition [12], chemical etching [13], and oxidation [14]. Among these approaches, oxidation-based methods are desirable due to their simplicity, low cost, and environmental friendliness. In this work, the controlled oxidations of Cu mesh to form $Cu(OH)_2$ microneedles were carried out to elucidate oil-water separation by tailoring both surface architecture and interfacial wettability[15].

MATERIALS AND METHOD

Fabrication of $Cu(OH)_2$ coated mesh

Raw materials: sodium hydroxide (NaOH) pellets, ammonium persulphate ($(NH_4)_2S_2O_2$) powder, absolute ethanol, stearic acid, and acetone were used as received. A commercially available Cu mesh (80 mesh number) was first ultrasonically cleaned, then sequentially rinsed with acetone and deionized water for 15 min. An aqueous solution of 2.0 M NaOH and 0.13 M $(NH_4)_2S_2O_8$ was prepared. The Cu mesh was immersed in the solution for varying durations (10, 20, 30, and 40 min), then rinsed thoroughly with deionized water and dried in an oven at 70 °C for 30 min. The obtained $Cu(OH)_2$-coated meshes were used directly for characterisation and oil-water separation tests.

Characterizations

The surface morphology of the Cu mesh was characterized using a scanning electron microscope (SEM, Tescan Vega) equipped with an energy-dispersive X-ray spectroscopy (EDX) system for elemental analysis. SEM images were acquired at an accelerating voltage of 20 kV, beam current of 30 pA, and working distance of 10 mm. Detailed $Cu(OH)_2$ structural features were examined at 20,000× magnification. The average length and width of the needle-like $Cu(OH)_2$ structures were calculated from SEM images using

ImageJ image processing software. The structure and phase composition of each sample were determined using an X-ray diffractometer (XRD, Rigaku SmartLab SE). Step-scan XRD patterns were collected with 2θ ranging from 5° to 80°, a step size of 0.01°, and a scan speed of 3.00°/min, using Cu Kα radiation at 40 kV and 30 mA. The wettability of the mesh was evaluated using a contact angle goniometer (Ossila) equipped with a 1920×1080-pixel camera and a maximum measurement speed of 33 ms. For each contact angle, 5 µL of water and oil were dispensed, in triplicate, at different spots on the sample.

Separation of oil-water mixture

To evaluate the oil-water separation performance of the $Cu(OH)_2$/Cu mesh under practical conditions, oil-water mixtures (1:1 v/v) were prepared using oils with a wide range of viscosities. Four representative oils were selected, namely **c**yclohexane, diesel, olive oil, and engine oil (Table 1), covering viscosities from light to heavy. Cyclohexane and diesel were chosen to represent light and intermediate-viscosity hydrocarbons typically encountered in oil and gas effluents, while olive oil was included as an intermediate-viscosity oil relevant to agri-food wastewater. Engine oil, with the highest viscosity, was used to mimic heavy lubricating oils that require more demanding separation challenges. All selected oils are non-polar and degrade slowly.

The separation experiments were performed using a custom-built, gravity-driven setup (Figure 1). Before separation, the oil-water mixture was introduced into the apparatus, where the $Cu(OH)_2$/Cu mesh was placed horizontally inside a glass tube inclined at 10°, thereby allowing evaluation of the mesh's separation efficiency across the full viscosity range.

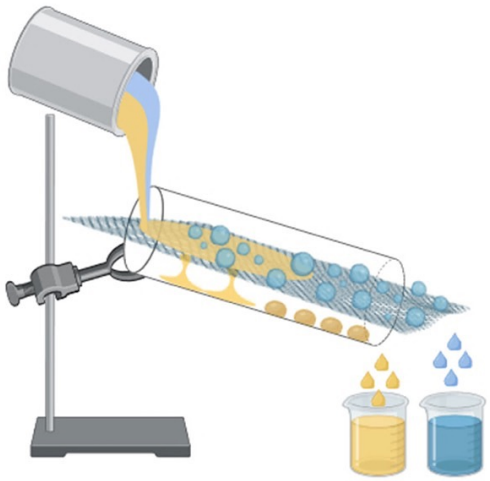

Figure 1. Setup for oil-water separation test

Table 1. Kinematic viscosities of selected oils for the oil-water separation test

Fluid	Kinematic viscosities (mm^2/s)
Cyclohexane	1.03
Diesel	2.00-6.00
Olive oil	43.20
Engine oil	65.00

The separation process was recorded in real time to determine the permeation flux, F of the Cu mesh [16], which was calculated using Eq. (1):

$$F = \frac{V}{S \times T} \quad (1)$$

where v represents the volume of permeated oil, s is the effective permeation area of the mesh, and T is the separation time. The oil-water separation efficiency, η [17] was calculated using Eq. (2):

$$\eta = \left(1 - \frac{C}{C_0}\right) \times 100\% \quad (2)$$

where C_0 and C denote the oil concentrations before and after separation, respectively. The use of oils with systematically increasing viscosity enables evaluation of the influence of viscous resistance on permeation flux and separation efficiency, as higher-viscosity oils experience greater flow resistance through the mesh pores, resulting in reduced permeation rates.

RESULTS AND DISCUSSION

Scanning Electron Microscope and Energy Dispersive X-ray Analysis

Figure 2 illustrates the surface morphology of the $Cu(OH)_2$/Cu mesh prepared at different immersion times in NaOH, examined from (1) cross-sectional and (2) horizontal perspectives. The cross-sectional images reveal that high-aspect-ratio $Cu(OH)_2$ needle-like structures grow perpendicularly from the Cu mesh substrate, forming a vertically aligned microstructure. The formation of $Cu(OH)_2$ in alkaline medium proceeds via an oxidation reaction, as described by Eq. (3):

$$Cu_{(s)} + 4NaOH_{(aq)} + (NH_4)_2S_2O_{8\,(aq)} \rightarrow Cu(OH)_{2\,(s)} + 2Na_2SO_{4\,(aq)} + 2NH_{3\,(aq)} + 2H_2O_{(l)} \quad \text{(Eq. 3)}$$

During this process, the Cu surface is rapidly oxidized to Cu^{2+} by the oxidizing agent $(NH_4)_2S_2O_8$, which subsequently reacts with OH^- ions to form $Cu(OH)_2$. In the horizontal-view images, the $Cu(OH)_2$ needle-like structures remain distinct and well separated at their tips after immersion for 10 and 20 min. With increasing immersion time to 30 min, the needle tips begin to interconnect, resulting in a denser surface morphology. Further prolonging the immersion time to 40 min results in shorter but thicker $Cu(OH)_2$ needles, indicating a change in growth behaviour.

The development of these $Cu(OH)_2$ microstructures significantly increases the surface roughness of the Cu mesh. As summarized in Table 1, both the average length and width of the $Cu(OH)_2$ needles increase with immersion time, from 4.586 ± 0.061 μm to 8.100 ± 0.129 μm in length and from 109 ± 2.00 nm to 115 ± 1.00 nm in width. However, at an immersion time of 40 min, these values decrease slightly to 6.422 ± 0.084 μm and 111 ± 1.00 nm, respectively, which may be attributed to agglomeration and partial structural coarsening that limit further longitudinal growth.

EDX mapping was used to analyse the elemental distribution on the Cu mesh surfaces prepared at different immersion times. All samples primarily consist of Cu and O, with a consistently high Cu content, as summarised in Table 2. A gradual decrease in O content from 47.2% to 31.4% is observed with increasing immersion time. This trend is consistent with the SEM results, in which prolonged immersion in NaOH leads to the

growth, interconnection, and eventual agglomeration of $Cu(OH)_2$ needle-like structures. Structural coarsening at longer immersion times reduces the exposed hydroxide surface area, resulting in a lower detected O content. Further insight is provided by the Cu:O mass ratios derived from the EDX analysis. At immersion times of 10 and 20 min, the Cu:O ratios are closer to 1:1, suggesting incomplete formation of the hydroxide phase. In contrast, at longer immersion times of 30 and 40 min, the Cu:O ratios increase to approximately 2.3:1 and 2.1:1, respectively, approaching the theoretical value for $Cu(OH)_2$ (2.0:1 based on atomic weights), thereby indicating the predominant formation of $Cu(OH)_2$ at these conditions.

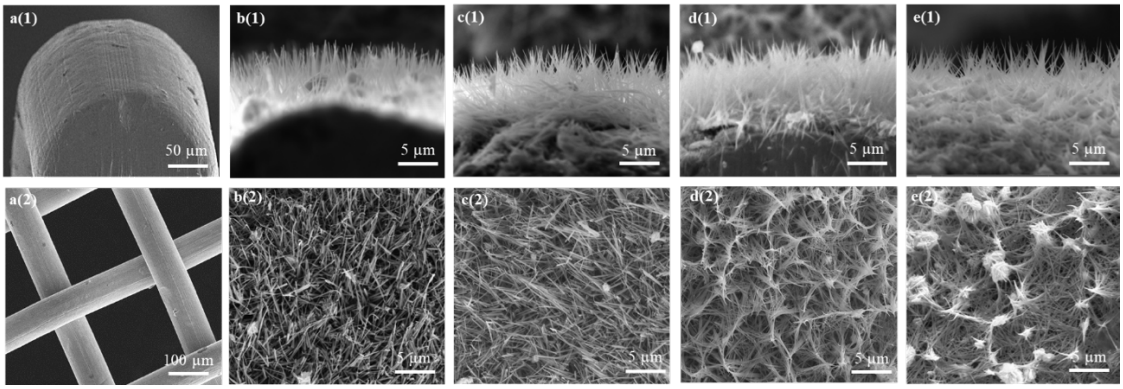

Figure 2. SEM images of Cu mesh and $Cu(OH)_2$/Cu meshes with different immersion times in NaOH: (a) bare Cu mesh, (b) 10 min, (c) 20 min, (d) 30 min and (e) 40 min

Table 2. Average length, average width, and element ratio of needle-like $Cu(OH)_2$ structure with different immersion times

Immersion time (min)	$Cu(OH)_2$ average length (µm)	$Cu(OH)_2$ average width (nm)	Mass of element (%)	
			Cu	O
Bare Cu mesh	-	-	100.0	-
10	4.586 ± 0.061	109 ± 2.00	50.6	47.2
20	5.605 ± 0.078	111 ± 1.00	51.2	47.3
30	8.100 ± 0.129	115 ± 1.00	72.6	27.4
40	6.422 ± 0.084	111 ± 1.00	66.6	31.4

X-ray Diffraction

XRD measurements were performed to complement the SEM and EDX analyses and to confirm the phase formation of $Cu(OH)_2$. As shown in Figure 3, the XRD patterns indicate that the dominant crystalline phase in all samples is cubic Cu (FCC structure, JCPDS No. 00-004-0836), denoted by the (●) symbol. The characteristic Cu diffraction peaks corresponding to the (111), (200), and (220) planes are observed in the bare Cu mesh and in all samples prepared at different immersion times, indicating the persistence

of the metallic Cu substrate. In addition to the Cu phase, diffraction peaks assigned to $Cu(OH)_2$ (orthorhombic structure, JCPDS No 01-072-0140), marked by the (♦) symbols, are detected and indexed to the (020), (021), (002), (111), (022), (130), and (132) planes. With increasing immersion time, the $Cu(OH)_2$ peaks become more pronounced, indicating progressive growth and increased crystallinity of the $Cu(OH)_2$ layer on the Cu mesh surface.

The marginal broadening of the $Cu(OH)_2$ full-width at half-maximum (FWHM) peaks indicates the presence of fine microneedles that grow via room-temperature oxidation. To quantify the crystallinity of the $Cu(OH)_2$ phase, the crystallite size was calculated using the Scherrer equation applied to the (020) and (002) reflections. The average crystallite size was approximately 0.1274 nm. This confirmed that the observed peak broadening results from the microcrystalline nature of the $Cu(OH)_2$ rather than from amorphous character. This trend is consistent with SEM observations and the bright blue colour, confirming that prolonged immersion promotes the formation of $Cu(OH)_2$ microstructures. Such delicate microneedle structures and OH functional groups are preferred for interfacial wettability in selective oil-water separation. However, the $Cu(OH)_2$ phase would be lost upon high-temperature annealing, resulting in the formation of CuO [18, 19].

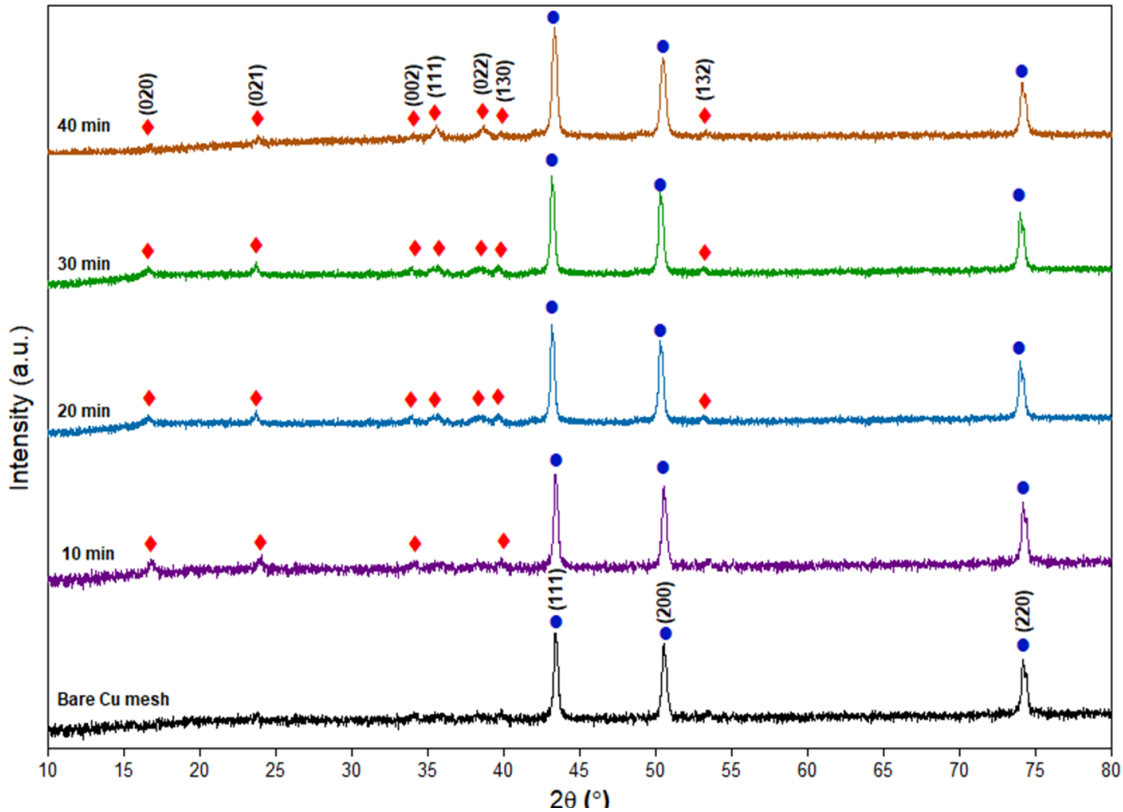

Figure 3. XRD patterns of Cu mesh with different immersion times

Contact Angle Measurement

Contact angle measurements were conducted to evaluate the wettability of the $Cu(OH)_2$/Cu mesh, and the corresponding water contact angle (WCA) and oil contact angle (OCA) as a function of immersion time are shown in Figure 4. The bare Cu mesh

exhibits a WCA of 132.93 ± 0.50°, indicating an intrinsically hydrophobic surface. With the formation of $Cu(OH)_2$ needle-like structures, the WCA increases to 139.89 ± 0.52° and 146.12 ± 0.72° for immersion times of 10 and 20 min, respectively. The WCA reaches a maximum value of 155.75 ± 0.77° at 30 min of immersion, corresponding to a superhydrophobic surface.

This enhancement in water repellency is consistent with the Cassie–Baxter wetting regime, in which the high-aspect-ratio $Cu(OH)_2$ microneedles trap air pockets beneath the water droplet, reducing the solid–liquid contact area and thereby preventing water permeation through the mesh [20, 21]. Such water-repellent behaviour is critical for oil-water separation, as it suppresses water penetration while maintaining open pathways for oil transport. When the immersion time is extended to 40 min, the WCA decreases to 145.78 ± 0.67°, attributable to structural agglomeration observed in the SEM images that disrupts the hierarchical roughness and compromises water repellence.

The oleophilic nature of the $Cu(OH)_2$/Cu mesh is also illustrated in Figure 3, where the oil contact angle decreases from 28.73 ± 0.64° for the bare Cu mesh to 19.45 ± 0.59°, 19.50 ± 0.64°, 17.52 ± 0.64°, and 18.87 ± 0.36° with increasing immersion time. The low OCA values indicate strong oil affinity, allowing oil droplets to readily wet and permeate the mesh under gravity. The combination of high WCA and low OCA achieved at an immersion time of 30 min provides an optimal wettability contrast, which is essential for achieving high separation efficiency and permeation flux. Therefore, the $Cu(OH)_2$/Cu mesh immersed for 30 min is selected for subsequent oil-water separation experiments.

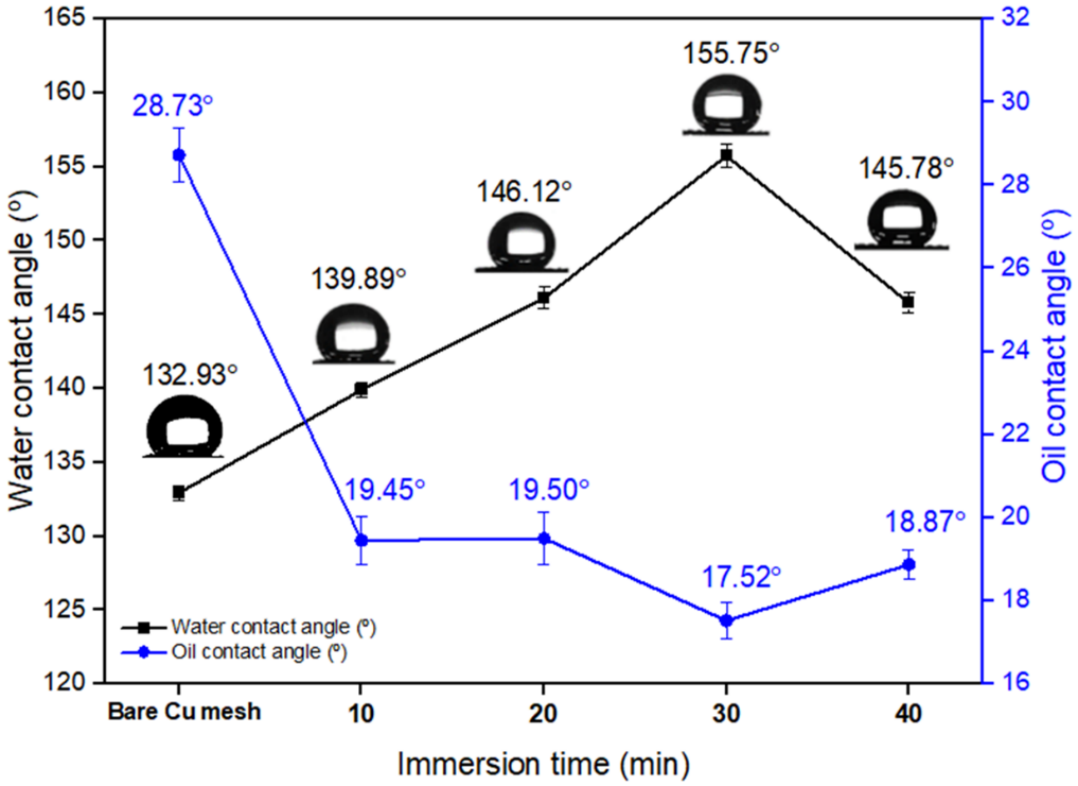

Figure 4. Water contact angle (WCA) and oil contact angle (OCA) of $Cu(OH)_2$/Cu meshes as a function of immersion time in NaOH

Oil-water Separation

To evaluate the oil-water separation performance, the oil-water mixture was introduced from the upper end of the tube, allowing gravity to drive the flow towards the $Cu(OH)_2$/Cu mesh. As the mixture passed through the inclined tube, the mesh selectively allowed oil to permeate while repelling water, and the separated oil and water were collected in two beakers positioned at the lower end of the apparatus. The separation efficiency and permeation flux for engine oil, diesel, olive oil, and cyclohexane are summarised in Figure 5.

Cyclohexane exhibits the highest separation efficiency of 98.10%, attributable to its low viscosity and reduced flow resistance. Oils with intermediate viscosities, such as diesel and olive oil, show slightly lower separation efficiencies of 96.20% and 94.46%, respectively. In contrast, engine oil, the most viscous among the selected oils, yields the lowest efficiency of 92.77%. A similar viscosity-dependent trend is observed for the permeation flux. Cyclohexane achieves the highest flux of 1648.65 $kg \cdot h^{-1} \cdot m^{-2}$, whilst engine oil exhibits the lowest flux of 842.86 $kg \cdot h^{-1} \cdot m^{-2}$, with diesel and olive oil displaying intermediate values of 1163.64 $kg \cdot h^{-1} \cdot m^{-2}$ and 865.04 $kg \cdot h^{-1} \cdot m^{-2}$, respectively.

The permeation behaviour can be interpreted using a Darcy-type flow model [22], where the flux is inversely proportional to the oil viscosity under a constant gravitational driving force. In addition to viscosity effects, the high-aspect-ratio $Cu(OH)_2$ microneedle structures play a critical role in regulating oil transport through the mesh. These vertically aligned microstructures increase the effective surface area and create interconnected microchannels that promote oil spreading and continuous flow, while simultaneously maintaining water repellence. As a result, the hydraulic resistance experienced by low-viscosity oils is minimised, enabling high permeation flux. Conversely, higher-viscosity oils experience increased resistance within the structured surface, leading to reduced flux. The combined influence of oil viscosity and high-aspect-ratio surface architecture governs the overall separation performance of the $Cu(OH)_2$/Cu mesh.

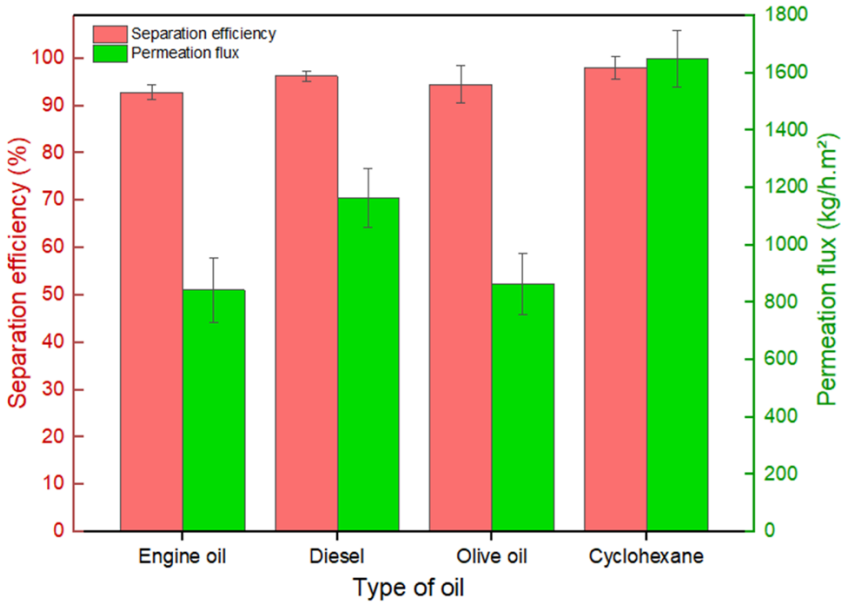

Figure 5. Separation efficiency and permeation flux for different types of oils

CONCLUSIONS

In summary, a $Cu(OH)_2$/Cu mesh was successfully fabricated via a simple immersion process, with an optimal immersion time of 30 min. Under these conditions, high-aspect-ratio $Cu(OH)_2$ needle-like structures with interconnected tips were formed, exhibiting an average length of 8.10 μm and a width of 115 nm. The resulting $Cu(OH)_2$/Cu mesh demonstrated pronounced superhydrophobic–oleophilic behaviour, achieving a maximum water contact angle of 155.75° and a low oil contact angle of 17.52°. Owing to the favourable surface architecture and wettability, the optimised mesh showed excellent oil-water separation performance, with a separation efficiency of up to 98.10% and a high permeation flux of 1648.65 $kg \cdot h^{-1} \cdot m^{-2}$. Notably, the use of a facile, cost-effective, and chemically efficient immersion process underscores the scalability and sustainability of this approach for large-area fabrication and practical wastewater treatment.

ACKNOWLEDGEMENTS

We thank Universiti Malaysia Terengganu for providing funding support for this project (UMT/TAPE-RG/2022/55388).

AUTHORS' CONTRIBUTIONS STATEMENT

The manuscript was written through the contributions of all authors. All authors have approved the final version of the manuscript. O.J.L. and M.A.B designed and organized this work. O.J.L., M.A.B., N.A.Z.N.M., and F.D. fabricated and characterized the meshes and conducted the oil-water separation tests. M.A.B., M.S.M.G. and N.S.M.S performed SEM and conducted water/oil contact angle measurement.

CONFLICT OF INTEREST

The authors declare that they have no known competing financial interests or personal relationships that could have influenced the work reported in this paper.

REFERENCES

1. Zhu M, Liu Y, Chen M, Xu Z, Li L, Zhou Y. Metal mesh-based special wettability materials for oil-water separation: A review of the recent development. *Journal of Petroleum Science and Engineering.* 2021;205: 108889.
2. Zhang N, Qi Y, Zhang Y, Luo J, Cui P, Jiang W. A review on oil/water mixture separation material. *Industrial & Engineering Chemistry Research*. 2020; 59(33):14546-68.
3. Lü X, Lin H. Facile fabrication of robust superhydrophobic/superoleophlic Cu coated stainless steel mesh for highly efficient oil/water separation. *Separation and Purification Technology*. 2021;256:117512.

4. Gulfam R, Zhang P. Fabrication and characterization of fluffy mono-coated copper meshes and their applications for oil/water separation. *Colloids and Surfaces A: Physicochemical and Engineering Aspects*. 2021;625:126883.
5. Deng L, Gong H, Shen X, Yu F, Zheng Y, Wang S. Poly (ionic liquid)-coated $Cu(OH)_2$ nanoneedle mesh with corrosion resistance for oil/water separation. *Journal of Environmental Chemical Engineering.* 2025;13(2):115675.
6. Huang Z, Wang Z, Wang S, Shan X, Yin S, Tao B. Superhydrophilic–superhydrophobic integrated system based on copper mesh for continuous and efficient oil–water separation. *RSC Advances*. 2024;14(9):6064-71.
7. He J, Li J, Ma L, Pang Y, Liu L, Liu Q, Peng L, Qu M. High-flux oil–water separation with superhydrophilicity and underwater superoleophobicity ZIF-67@$Cu(OH)_2$ nanowire membrane. *Journal of Materials Science*. 2021;56(4):3140-54.
8. Wang M, Zhang Z, Wang Y, Zhao X, Men X, Yang M. Ultrafast fabrication of metal–organic framework-functionalized superwetting membrane for multichannel oil/water separation and floating oil collection. *ACS Applied Materials & Interfaces.* 2020;12(22):25512-20.
9. He H, Li Z, Ouyang L, Liang Y, Yuan S. Hierarchical WO3@ $Cu(OH)_2$ nanorod arrays grown on copper mesh with superwetting and self-cleaning properties for high-performance oil/water separation. *Journal of Alloys and Compounds.* 2021;855:157421.
10. Luo ZY, Wang D, Chen KX, Huang L, Liu X, Zhang Q, Zhu H, Zhu S. Metal oxy-hydroxides with a hierarchical and hollow structure for highly efficient solar-thermal water evaporation. *ACS Applied Materials & Interfaces*. 2021;13(23):27726-33.
11. Barthwal S, Barthwal S, Singh B, Singh NB. Multifunctional and fluorine-free superhydrophobic composite coating based on PDMS modified MWCNTs/ZnO with self-cleaning, oil-water separation, and flame retardant properties. *Colloids and Surfaces A: Physicochemical and Engineering Aspects*. 2020;597:124776.
12. Hou Y, Peng Z, Liang J, Fu S. Facile preparation of petaliform-like superhydrophobic meshes via moisture etching for oil-water separation. *Surface and Coatings Technology*. 2020;399:126124.
13. Le TT, Hoang TB. Fabrication of Superhydrophobic copper using via chemical etching and modification route. *JST: Engineering And Technology For Sustainable Development*. 2022;32(4):1-8.
14. Zhou B, Bashir BH, Liu Y, Zhang B. Facile construction and fabrication of a superhydrophobic copper mesh for ultraefficient oil/water separation. *Industrial & Engineering Chemistry Research.* 2021;60(22):8139-46.
15. Yuan J, Cui C, Qi B, Wei J, Qaisrani MA. Study on oil-water separation of selective-wettability meshes with different Micro/Nano structures. *Colloids and Surfaces A: Physicochemical and Engineering Aspects*. 2020;584:124026.
16. Chen YL, Shao W, Zhong XF, Yang SY, Xu ZM, Sun JJ, Chen GJ, Zhang PP, Li Y, Xue M. Rapid electrochemical fabrication of MOF-coated mesh membranes with complementary wettability for high-efficiency oil-water separation. *Journal of Hazardous Materials.* 2025;500:140392.
17. Zhan Y, Liu C, Li X, Yongqiang F, Jinglong J, Jin X. Fabrication of under liquid dual superlyophobic ZnOHF@SSM film for oil/water emulsion separation. *Journal of Environmental Chemical Engineering.* 2025;13(6):119968.

18. Mahana D, Mauraya AK, Singh P, Muthusamy SK. Evolution of CuO thin films through thermal oxidation of Cu films prepared by physical vapour deposition techniques. *Solid State Communications.* 2023;366:115152.
19. Lu C, Qi L, Yang J, Zhang D, Wu N, Ma J. Simple template-free solution route for the controlled synthesis of $Cu(OH)_2$ and CuO nanostructures. *The Journal of Physical Chemistry B*. 2004;108(46):17825-31.
20. Wang Y, Liu P, Luo R, Chen B, Li J, Yang F, Zhou H, Zeng J, Xing L, Guo J. Design and fabrication of superhydrophobic photothermal coating on copper mesh and its applications on anti-corrosion, anti-icing and oil-water separation. *Progress in Organic Coatings*. 2024;188:108243.
21. Ma R, Li R, Niu Q, Zeng Y, Li J, Bai S, Cheng Y. Preparation of superhydrophobic surfaces based on copper mesh substrates and its application performance. *ACS Omega*. 2023;8(48):45616-25.
22. Lichade KM, Deshpande AA, Pan Y. 3D printing of hierarchical porous structures for oil/water separation and absorption. *ACS Applied Polymer Materials.* 2025;7(17):11425-11435